AD-A183 329 CHARGE TRANSFER DEVICE DETECTORS FOR ANALYTICAL OPTICAL SPECTROSCOPY - OP (U) ARIZONA UNIV TUCSON DEPT OF CHEMISTRY R B BILHORN ET AL 26 MAY 87 TR-49 1/1

UNCLASSIFIED N00014-86-K-0316 F/G 20/6 NL

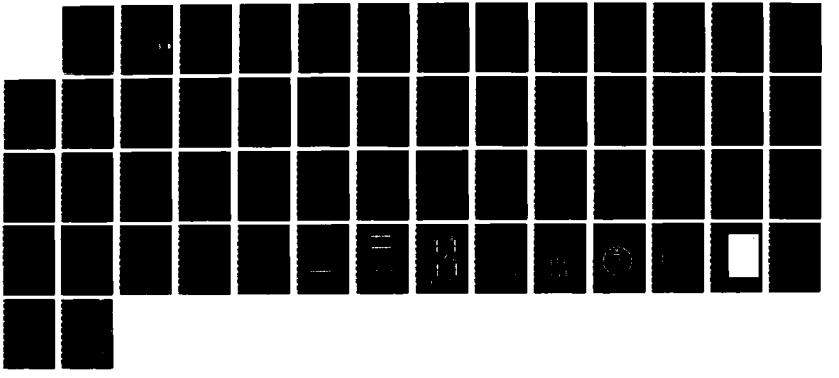

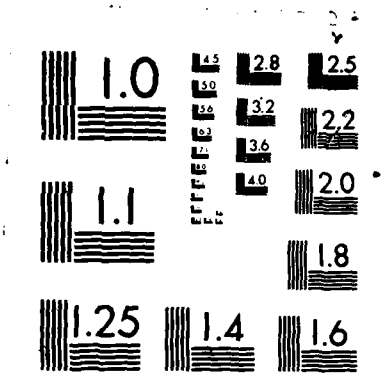

(12)

SECURITY CLASSIFICATION OF THIS PAGE (When Data Entered)

REPORT DOCUMENTATION PAGE

READ INSTRUCTIONS BEFORE COMPLETING FORM

1. REPORT NUMBER	2. GOVT ACCESSION NO.	3. RECIPIENT'S CATALOG NUMBER
49		

4. TITLE (and Subtitle)

Charge Transfer Device Detectors for Analytical Optical Spectroscopy - Operations and Characteristics

5. TYPE OF REPORT & PERIOD COVERED

Interim

6. PERFORMING ORG. REPORT NUMBER

7. AUTHOR(s)

R.B. Bilhorn, J.V. Sweedler, P.M. Epperson, and M.B. Denton

8. CONTRACT OR GRANT NUMBER(s)

N00014-86-K-0316

9. PERFORMING ORGANIZATION NAME AND ADDRESS

Department of Chemistry
University of Arizona
Tucson, AZ 85721

10. PROGRAM ELEMENT, PROJECT, TASK AREA & WORK UNIT NUMBERS

NR 051-549

11. CONTROLLING OFFICE NAME AND ADDRESS

Office of Naval Research
Arlington, Virginia 22217

12. REPORT DATE

May 26, 1987

13. NUMBER OF PAGES

51

14. MONITORING AGENCY NAME & ADDRESS (if different from Controlling Office)

15. SECURITY CLASS. (of this report)

Unclassified

15a. DECLASSIFICATION/DOWNGRADING SCHEDULE

16. DISTRIBUTION STATEMENT (of this Report)

This document has been approved for public release and sale; its distribution is unlimited.

17. DISTRIBUTION STATEMENT (of the abstract entered in Block 20, if different from Report)

18. SUPPLEMENTARY NOTES

Submitted for publication to Applied Spectroscopy.

19. KEY WORDS (Continue on reverse side if necessary and identify by block number)

Spectroscopic detectors, Charge transfer devices, Charge-coupled device, Charge injection device, Optical spectroscopy.

20. ABSTRACT (Continue on reverse side if necessary and identify by block number)

This article is the first in a two part series describing the operation, characteristics and application of a new class of solid-state multichannel UV-visible detectors. In this manuscript, Charge Transfer Devices (CTDs) are described. Detector characteristics pertinent to spectroscopic application including quantum efficiency, read noise, dark count rate and available formats are emphasized. Unique capabilities such as the ability to non-destructively read out the detector array, and the ability to alter the effective detector element size by a (Continued on other side)

DD FORM 1 JAN 73 1473 EDITION OF 1 NOV 65 IS OBSOLETE
S/N 0102-LF-014-6601

SECURITY CLASSIFICATION OF THIS PAGE (When Data Entered)

20. Abstract (continued)

process called binning are described. CTDs with peak quantum efficiencies over 80% and significant responsivity over the wavelength range of 0.1 nm to 1100 nm are discussed. Exceptionally low dark count rates which allow integration times up to many hours and read noises more than two orders of magnitude lower than commercially available PDA detectors both contribute to the outstanding performance offered by these detectors.

OFFICE OF NAVAL RESEARCH

Contract N00014-86-K-0316

Task No. 051-549

TECHNICAL REPORT NO. 49

Charge Transfer Device Detectors for Analytical Optical Spectroscopy - Operations and Characteristics

by

R.B. Bilhorn, J.V. Sweedler, P.M. Epperson, and M.B. Denton

Prepared for publication in

Applied Spectroscopy

Department of Chemistry
University of Arizona
Tucson, Arizona 85721

May 26, 1987

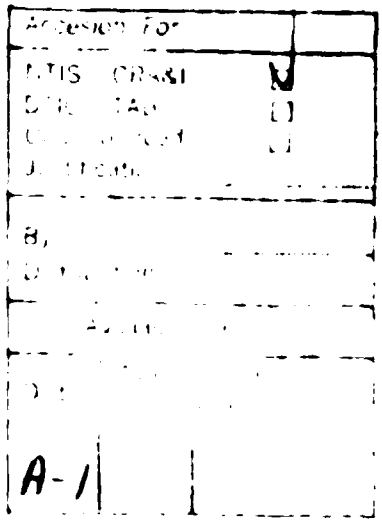

Charge Transfer Device Detectors for Analytical Optical Spectroscopy- Operation and Characteristics

by

R.B. Bilhorn, J.V. Sweedler, P.M. Epperson, and M.B. Denton

Chemistry Department, University of Arizona

Tucson, Az 85721

Abstract

This article is the first in a two part series describing the operation, characteristics and application of a new class of solid-state multichannel UV-visible detectors. In this manuscript, Charge Transfer Devices (CTDs) are described. Detector characteristics pertinent to spectroscopic application including quantum efficiency, read noise, dark count rate and available formats are emphasized. Unique capabilities such as the ability to nondestructively read out the detector array, and the ability to alter the effective detector element size by a process called binning are described. CTDs with peak quantum efficiencies over 80% and significant responsivity over the wavelength range of 0.1 nm to 1100 nm are discussed. Exceptionally low dark count rates which allow integration times up to many hours and read noises more than two orders of magnitude lower than commercially available PDA detectors both contribute to the outstanding performance offered by these detectors.

Index Headings: Spectroscopic detectors, Charge transfer devices, Charge-coupled device, Charge injection device, Optical spectroscopy.

Introduction

Optical spectroscopic methods of analysis are powerful and versatile techniques widely employed by the modern analytical chemist. Spectroscopic measurements based on absorption, fluorescence and emission offer both selectivity and sensitivity. Recent improvements in optical radiation detector technology, particularly the advent of high performance multichannel detectors, are expected to make spectrochemical methods of analysis even more widely applicable.

Relatively little has changed in the way optical radiation has been detected in analytical spectroscopy for many years. Photomultiplier tubes have been used almost exclusively for the detection of photons in the UV, visible and near IR spectral regions. PMTs have very high and almost noiseless internal gain and for this reason, previous detector technologies have not been able to match PMT performance. Some new multichannel alternatives to PMT detection are capable of comparable sensitivity and dynamic range, when compared on a detector element by detector element basis. The multichannel advantages offered by these detectors are expected to be a great boon to analytical spectroscopy.

The PMT is a relatively sensitive low noise detector so that in the typical absorption, emission or luminescence measurement the amount of light required (or, under constant flux conditions, the length of time required) to make an intensity measurement which is dominated by source noise (fluctuation) or photon noise, rather than by detector noise, is relatively short. An ultraviolet-visible spectrum of moderate resolution and which is not dominated by detector noise is easily acquired in a few minutes on a scanning instrument

employing a PMT. This technology has limitations however. Spectral acquisition time limitations imposed by the transient nature of a species of interest, or light throughput limitations imposed by micro-sampling (eg. high performance liquid chromatography detectors), push the technology of sequential multiwavelength, ultraviolet-visible instrumentation near to, if not beyond, the point of inadequate performance.

Multichannel techniques, which allow measurement of each wavelength interval during the entire allotted measurement time, offer potential signal to noise improvements over sequential approaches. For multiple PMT detectors or multichannel detectors, where each detector element is capable of the same performance as a single PMT detector, the improvement in signal to noise ratio considering only the reduction in photon noise, is proportional to $N^{1/2}$ where N is the number of PMTs or detector elements. This result applies in general when photon shot noise dominates. In regions of the spectrum where this type of noise is of major importance, multichannel detection should be preferable as compared to sequential detection any time light intensity measurements are to be made over more than one wavelength interval.

The recent appearance of commercial instrumentation employing photodiode arrays (PDAs) for ultraviolet-visible absorption spectrometry has provided an alternate technology for the measurement of ultraviolet-visible absorption spectra in short time periods. Although an individual photodiode in a PDA is not as good a detector as a PMT, under some circumstances the multichannel advantage outweighs the disadvantage of the poorer detector. Additionally, the reliability inherent in a PDA spectrometer as compared to a moving mirror rapid scanning spectrometer is a considerable advantage. Ultraviolet-visible absorption spectrometers employing PDAs do not offer the

performance of sequential instruments when time/light/scanning speed is not a limiting factor. Also, this technology has not been as successful in other types of analytical spectroscopy (luminescence, Raman, and atomic emission) as it has been in absorption spectroscopy because these spectroscopies require better sensitivity at low light levels.

Until very recently, no multichannel detector has offered the sensitivity, dynamic range and noise performance necessary to make it competitive with the PMT. For this reason, successful application of multichannel or multiplexed detection has been limited to those experimental conditions where the multichannel and/or multiplex advantages outweigh the noise and dynamic range disadvantages which had been characteristic of these detectors. This manuscript is a review of the theory, design, operation and performance of a relatively new class of multichannel light detectors. These detectors are termed charge transfer devices (CTDs) and currently, some of these detectors exceed the sensitivity and dynamic range capabilities of all other types of light detectors.

Application of CTDs for spectroscopy and scientific imaging has taken place mostly in the fields of astronomy and astrophysics, with a few more recent applications being reported in microscopy. The performance of CTDs has advanced to the point where the time is ripe for the introduction of this new technology to the field of analytical chemistry. It is expected that the adaptation of this technology to analytical spectroscopy will produce the same improvements in levels of performance that have been obtained in astronomy. The second article in this series describes the parameters which affect the ultimate sensitivity that can be obtained by a spectroscopic system employing

a CTD detector, as well as several analytical spectroscopic applications of these detectors.

CTDs are available in a wider variety of formats than any other spectroscopic detector. CTD sizes range from a single element detector with a 1 mm^2 photoactive area to a 2048 by 2048 detector element array with a photoactive area of over 3000 mm^2. These detectors are not susceptible to the read-out droop associated with PDAs, so the quality of an image is maintained from the first detector element to the last. CTDs can have peak quantum efficiencies over 80%, and significant responsivity over the wavelength range from 0.1 nm to 1100 nm. In addition, low dark count rates which allow integration times of as long as several hours and read noises more than two orders of magnitude lower than commercially available PDA detectors, both contribute to the outstanding low light level performance obtainable from these detectors.

Charge Transfer Devices

CTDs are solid state integrating multichannel photon detectors which employ inter-cell or intra-cell charge transfer for readout. These detectors are integrating detectors which accumulate signal information as light strikes them much like photographic film. This is in contrast to photomultiplier tubes which produce a signal current in proportion to the instantaneous photon flux at the photocathode. CTDs are solid-state integrated circuits produced by conventional VLSI photo-fabrication techniques. Although CTDs have been produced from a number of semiconductor materials, this report will only consider devices based on silicon technology.

The accumulated signal information in a CTD is stored as electrical charge, the amount of photogenerated charge being in proportion to the number of photons striking the detector. The amount of charge generated is measured either by moving it from the detector element where it was accumulated to a charge sensing amplifier (inter-cell charge transfer) or by moving it within a detector element and sensing voltage changes induced by the movement (intra-cell charge transfer). The method of charge information readout gives rise to the two types of CTDs, the charge-coupled device (CCD), employing inter-cell charge transfer readout, and the charge injection device (CID), employing intra-cell charge transfer readout.

Since their introduction in the early 1970s, CIDs and CCDs have undergone a number of refinements and improvements which have not been widely followed in the chemical literature. It is the intent of this report to present performance data for a number of modern CTDs. Before this discussion can be undertaken however, the operating principles of CIDs and CCDs need to be reviewed so that the implications of the differences in their architecture can be fully appreciated. More complete descriptions of the operation of particular sensors appear in the electrical and optical engineering literature and the interested reader is referred there for more complete descriptions (see for example refs. 1-4).

The Charge Injection Device

The CID is the result of one approach to making solid-state imagers that was undertaken by the General Electric Company. The first reports on imagers appeared in 1974. CIDs are metal-oxide-semiconductor integrated

circuits which have been fabricated in a variety of formats as shown in Table I.

An individual CID detector element consists of two electrically conductive polycrystalline silicon electrodes overlaying a thin silicon oxide and/or silicon nitride insulating layer. The insulator separates the electrodes from an N doped silicon region which is used for photogenerated charge storage. Devices which are currently being manufactured have this n-doped layer epitaxially grown over a p-doped silicon substrate.

The actual configuration and geometry of the electrodes and insulators used in CIDs has evolved since the introduction of the first imagers, however the operation of the various types can all be understood conceptually by considering the two electrodes to be adjacent to each other and of equal size. Figure 1 shows the topology and the cross section of a single detector element in this hypothetical CID. One of the electrodes is associated with a column conductor, and one is associated with a row conductor. These connections allow the access of a single detector element within the array. If the electrodes are biased negatively with respect to the epitaxial layer, a charge inversion region is created under the electrodes in the n-doped epitaxy. These charge inversion regions are energetically favorable locations for mobile holes (minority charge carriers) to reside. The promotion of an electron into the semiconductor conduction band, such as by absorption of a photon in the epitaxial layer, creates a mobile hole which can then migrate and be collected in the inversion region. The electron is conducted across the reverse-biased, epi-substrate junction. An electric field gradient extends outward from the location of the electrodes making the area directly under the insulator the most favorable place for positive charge to reside.

The first few holes created by photon absorption are stored in this location with subsequently formed holes being stored at greater and greater distances from the insulator. The charge containing capacity of a detector element is limited by the dimensions of the inversion region. These dimensions are determined by the size of the electrodes, the potentials applied to the electrodes, the insulator material and thickness, the epitaxial layer conductivity and thickness and a number of other parameters.[1] The actual geometry of a modern CID is shown in Fig. 2. Polycrystalline silicon strips are used to form both the electrodes and the electrode interconnections.

The degree to which the inversion regions are filled with charge as well as the way in which charge is moved during readout can be shown pictorially by the use of "potential well" diagrams (Fig. 1). In these figures, the "favorableness" of a region for the storage of charge is indicated by the depth of a potential well. Charge contained in the potential well is indicated by shading or by plus signs. Although charge is shown as filling up the wells from the bottom, it should be remembered that charge initially resides near the silicon-silicon dioxide interface and the wells fill outward from there. In Fig. 1, one electrode is held at a more negative potential than the other, making it more favorable for charge to accumulate under this electrode. Charge storage under this electrode proceeds until the well capacity is reduced to equal the capacity of the other well. At this point, charge storage under both electrodes is equally favorable and the detector element is said to be saturated. Beyond this point, additional charge will be stored under both electrodes but, due to the nature of the readout process used in the CID, this additional charge cannot be quantified. Upon continued addition of charge, a

point will be reached where no more charge can be contained in either potential well. Additional charge generated within the detector element is then discharged across the epitaxy-substrate junction[5,6].

Unlike other imaging detectors (vidicon tubes, photodiode arrays and some charge-coupled devices), CIDs are very resistant to migration of excess charge to adjacent detector elements (blooming). A condition is conceivable however, where illumination is so intense that charge cannot migrate across the epitaxy-substrate junction at a sufficient rate. In this case, migration of charge to adjacent detector elements also occurs. Resistance to blooming is a very significant feature of CIDs that makes them particularly interesting as spectroscopic detectors.

A number of readout schemes have been used with CIDs, all of which use manipulations of electrode potentials to effect movement of charge either from one electrode to the other or from the electrodes in a detector element into the substrate. A readout method which differs from the video rate method used by General Electric in their current machine vision CID cameras, and which has been successfully employed in our laboratories for high photometric accuracy as well as high signal-to-noise ratio in spectrochemical analysis, will be briefly described. Details of the hardware employed to achieve this operation have been presented elsewhere[7,8].

Photogenerated charge is collected under only one of the two electrodes in a detector element and is quantified by sampling the potential change induced on the other (sensing) electrode by the movement of the charge. The charge is shifted from the electrode where it was originally collected (for example, the column electrode in Fig. 1) to the sensing electrode inducing a potential change $dV = dQ/C$ where C is the capacitance of the MOS

capacitor formed by the sensing electrode and dQ is the amount of charge transferred (see Fig. 3). The readout scheme employs two measurements of the potential on the sensing electrode. The first measurement is made prior to charge movement and the second samples the potential after the charge is shifted. The difference is proportional to the quantity of charge stored.

The movement of charge in the CID is accomplished by driving the potential on the electrodes from their negative (with respect to the substrate) integrating (charge collecting) potentials to positive potentials which cause the collapse of the inversion regions. The collapse of the potential well under one electrode causes any charge contained there to migrate to the adjacent electrode (performed to read out a detector element). The collapse of the inversion regions under both electrodes results in the recombination of electron hole pairs and the elimination of charge from the detector element.

The readout sequence can be completed in one of two ways. After charge is shifted from the charge collection electrode to the charge sensing electrode and the second potential measurement made, the potential well under the charge collection electrode can be re-established causing the charge to migrate back to its original position. This results in a restoration of the detector element to its condition prior to charge information read out. Because no net change is made in the quantity or location of photogenerated charge, this read out procedure has been called the non-destructive read out (NDRO). The other option upon completion of the second measurement of the potential on the sensing electrode is to collapse the potential well under this electrode. This causes electron hole pair recombination and elimination of charge from the entire detector element (destructive read out, DRO).

Averaging the results of a number of NDROs introduces no photon noise and is only subject to the device read noise. As a result, this procedure can be employed for improving the SNR of a photon-flux measurement. By computer summation of a number of non-destructive reads of the charge information in a detector element, the read noise, or the noise introduced by the detector and associated electronics, can be reduced. This is similar to, but not the same as, conventional signal averaging. Averaging of multiple measurements of photon flux is subject to the shot and other noises in the photon stream in addition to the detector noise. If the read noise is a white or random noise source, then the noise is reduced in proportion to the square root of the number of NDROs performed. In practice, read noise can be reduced by over a factor of 10 by the process of averaging multiple NDROs.[9]

In current devices, individual CID detector elements are accessed through the action of two independent X and Y scanners. These scanners sequentially connect rows and columns to the output amplifier and the charge drive signal respectively as shown in Fig. 4. The two scanners are operated independently of each other so that any desired column and row can be selected. The detector element at the intersection of a selected row and column can be read either destructively or non-destructively. Application of the drive signal to a column causes the charge contained in a detector element anywhere along the column to migrate to the row electrode in that detector element. Only the charge information at the detector element which is at the intersection of the selected column and row is sensed because only that row is connected to the amplifier. The charge at all other columns remains under the column capacitors.

Application of a positive voltage to the selected row while the drive pulse is present on the selected column injects the charge from the detector element at the row and column intersection into the substrate. Charge at all other detector elements remains intact because either a row or a column potential well exists at these sites. In addition to the two scanners discussed above, modern CIDs have a scanner at the opposite end of the rows from the select scanner and a set of switches at the end of each column. These perform various functions such as simultaneously clearing the entire array of charge and reseting the normal (negative) potential on the columns used for charge collection.

Due to the nature of the multiplexed organization of the CID, the output capacitance appearing at the input of an off chip amplifier is relatively high as compared to a CCD. This is the capacitance on which the voltage change is induced by the movement of charge in a detector element, $dV = dQ/C$. A reduction in this capacitance increases the voltage change induced by a fixed amount of charge. Also, the dominant noise source in the CID is directly proportional to the capacitance appearing at the input node of the off-chip amplifier. Efforts are underway to reduce this capacitance in new CID's. The noise observed in current scientific CID systems is in the hundreds of charge carriers although this is reducible to under 100 carriers by employing NDROs.

Charge-Coupled Devices

The charge-coupled device concept was first introduced in 1970 by Boyle and Smith.[10,11] CCDs are available from a number of manufacturers and have been used in a variety of military, commercial and consumer imaging applications. A great deal of literature exists concerning the operating principles and fabrication of CCD imagers and a great deal of effort has been expended in optimizing CCDs for scientific imaging applications.[12] It is beyond the scope of this review to discuss in detail the evolution of sensor design and the wide variety of detectors that have been made or are currently being used. Rather, it is the intent of the authors to give a general overview of CCD operation so that later discussions of CCD merits relative to other detector technology will be understandable and discussions of design considerations for spectrochemical systems will be possible.

Like the CID, the CCD is a metal-oxide-semiconductor structure that stores photogenerated charge carrier packets. Unlike the CID however, CCDs are usually fabricated in p-type material so that electrons are stored. The charge packets can be transferred by the controlled movement of potential wells just as in the CID. The most significant difference between CIDs and CCDs is the way in which charge information is read out. The quantity of charge contained in a packet is measured in CCDs by shifting it to a reverse biased P-N junction capacitance and measuring the voltage change that is produced. A single output node is used at the edge of a linear or two dimensional array of detector elements and the charge from each detector element is shifted in sequence to this output. A reset switch establishes the potential of this diode prior to the introduction of the charge from a detector element and a MOS amplifier is usually integrated on the chip to sense the potential

change. It is the ability to transfer charge from a sensing element to a specialized low capacitance output node, and hence eliminate a high capacitance multiplexed architecture, that differentiates CCDs from CIDs and PDAs. The extremely small capacitance of the input node of this amplifier allows CCDs to achieve an ultra low read noise.

The transfer of charge from the detector element where it was collected to the output node occurs by shifting the charge from one detector element to the next, adjacent detector element. The potential wells in a detector element must be controllable in three independent regions in order to perform this transfer. Control over these three regions can be achieved in a number of ways, but the most easily visualized way is through the use of three separate electrodes and is shown in Fig. 5. At least one of the three potential well regions in a detector element is always collapsed in order to provide a barrier to separate charge packets that originate from adjacent detector elements. Shifting the location of this barrier causes charge to migrate due to a combination of fringe field drift and self-induced drift. Fringe field drift is caused by the existence of an electric field, in this case because of the potential difference between electrodes. Self-induced drift is due to a nonuniform distribution of electrons under two electrodes at the same potential.

The organization of a two dimensional CCD array is illustrated in Fig. 6. Columns are clocked in parallel, shifting all of the charge in the array one row at a time toward a serial transfer register. Once a row is shifted into the serial register, the charge from individual detector elements is shifted to the low capacitance output node. Fixed potential barriers are created between columns to prevent charge migration in this direction. These

barriers, or channel stops as they are also called, can be created either by a diffusion of p-type material or by using a thick oxide over the area of the channel stop.

The control over the three potential regions in a real CCD detector element can be achieved in a number of ways. Fewer than three electrodes can be used by employing p-type material implants or variations in oxide thickness to create steps in the potential wells which force the desired charge movement. These fixed potential barriers are just like those used in the formation of channel stops. Devices using only a single electrode (uniphase) and devices using two electrodes have been fabricated and are commercially available. Devices have also been fabricated with four electrodes rather than three for reasons of ease of manufacture. Representations of the four types of gate structure are illustrated in Fig. 7.

The transfer of charge from all detector elements in a CCD to a single output stage eliminates the multiplexing circuitry that is necessary in CIDs and PDAs. Because of this, the capacitive load associated with the output of a CCD can be very low, and hence the read noise is extremely low in these devices. On the other hand, extremely efficient transfer of charge from detector element to detector element as well as from the parallel register into the serial register and from the serial register into the output diffusion is a necessity. Minimal degradation of the signal information from a detector element after several thousand transfers requires charge transfer efficiencies (CTE) on the order of 0.99999. CTEs on the order of 0.999995 are achievable and devices with this level of performance have been produced.

CCD detectors have a unique capability which distinguishes them from other detectors. This is a readout mode where charge from more than one

detector element is combined on chip before being read out. The process, called "binning", involves moving the charge from a number of detector elements into a single element or "bin" and then transferring the charge from the bin to the output node. Charge from any number of consecutively arranged detector elements can be binned. The advantage of summing the analog signal on chip as opposed to digital summing in memory is that the summed charge is subject to only one read operation and thus has only the noise associated with one read, whereas digitally summing the data also adds the read noises from each element in quadrature. In extreme low light level situations where the dominant source of noise is detector read noise, the summing in computer memory is noisier by a factor equal to the square root of the number of summed elements. Binning can be considered as a way of dynamically altering the "grain size" of the solid state "photographic emulsion" and correspondingly altering the "photographic speed" of the device. In spectroscopy, the ability of the CCD to bin charge from multiple detector elements allows one to increase the sensitivity of a measurement. Some resolution loss is incurred, however because of the large number of original resolution elements in the CCD arrays, this resolution loss may not be significant.

As was mentioned earlier, CCDs are available with a wide variety of detector sizes, number of detector elements, and geometries. Table I lists the formats of a large number of CCDs, the manufacturers, and comments pertaining to their use as detectors for spectroscopic applications. Figure 8 is a photograph of many of the CTD detectors evaluated in our laboratories. Because of the large variety of available detectors, devices can be selected for specific applications matching device performance to experimental requirements.

CTD Performance Characteristics Influencing Analytical Spectroscopy

Many of the performance characteristics of a given CCD are dependent on the method used in its operation. For example, the same CCD used in a commercially available video camera and in a scientific camera will have a much different level of performance. Video cameras employing CCDs operate at approximately sixty frames per second. At this high read rate, the sensors can be operated at room temperature with no ill effects from dark current. The high bandwidth of video rate preamplifiers makes these cameras significantly noisier than CCD cameras designed for scientific applications. Scientific cameras operate at much lower frame rates (e.g., several seconds) and employ cooling to reduce dark current as well as very low noise amplifiers and signal conditioning circuits. The performance characteristics given in this manuscript are for CTDs operated in optimized scientific detector systems. Table II is a summary of the spectroscopically pertinent electro-optical characteristics of several CTDs.

Quantum Efficiency

The intrinsic quantum efficiency of all silicon detectors (PDAs, CTDs, etc.) is high compared to the quantum efficiency of available photocathode materials. Silicon CTDs can have sign icant response from the soft x-ray to the near infrared spectral region.[13] The responsivity of a CTD detector to light at various wavelengths depends on several processes, including losses due to reflection, losses due to absorption in regions where electron hole pairs are not collectable, and non-unity efficiency of collection of carriers created in regions where they should in theory be collectable. Charge collection efficiencies (CCE) approaching 100% are possible in devices where defects

which allow electron hole pair recombination are minimized, and where structures have been added to force charge collection in the desired regions.[13] Thus, losses due to poor charge collection efficiency are not a problem in modern scientific CTDs.

While the intrinsic quantum efficiency of the bulk silicon is similar in the different types of detectors, the overall quantum efficiencies of the indivdual manufacturers' CTDs and PDAs are very different depending on the cross sectional geometry, the fabrication methods and materials. For example, several CCDs have quantum efficiencies over 10% only in the 350-900 nm wavelength range, while others have a usable wavelength range from 0.1-1000 nm. Two regions exist where photons can be absorbed but which do not produce collectable carriers. The first of these is in the gate structure on the surface of the CTD. Photons which are absorbed by the electrodes or the insulators are lost and result in a decrease in the *apparent quantum* efficiency of the device. In addition, photons which penetrate the CTD entirely or which are absorbed outside of the region into which the potential gradients extend are also lost. As an example, photons absorbed in the substrate of devices fabricated in epitaxial silicon are not detected. The greater characteristic absorption depth of longer wavelength photons in silicon makes them more likely to penetrate beyond a region where absorption will produce collectable carriers[14]. Additionally, as the energy of the photons approaches the band gap of the semiconductor, the probability of electron hole pair production decreases. For this reason, the quantum efficiency of CTDs generally decreases at longer wavelengths until the photons no longer carry the necessary energy to generate electron hole pairs (~1.1 μm).

The greater absorption coefficients for blue and ultraviolet photons (as compared to longer wavelength visible photons) in polysilicon and silicon dioxide result in reduced quantum efficiency in this region of the spectrum for devices having greater overlaying gate structure. Device architectures which minimize the amount of gate structure on the imager surface (uniphase CCDs) tend to have better quantum efficiencies in this region. Devices which are designed to be illuminated from the surface opposite from the surface on which the gates are constructed offer the greatest freedom from losses due to absorption. These backside illuminated devices must be thinned however, (a difficult and hence expensive process) so that photons entering the device will be absorbed in regions where the generated electron hole pairs can be collected. Thinning is a chemical etching process by which a typical integrated circuit wafer thickness is reduced to between 5 and 20 micrometers. The absorption depth of photons in silicon varies from tens of angstroms for vacuum ultraviolet and ultraviolet photons to tens of micrometers for red and near infrared photons. Thinned CCDs therefore have poorer responsivity in the near infrared region of the spectrum than thick front side illuminated devices but respond very well to wavelengths as low as 0.1 nm.[13]

Reductions in CTD responsivity can also be due to reflection at the surface of the imager. The relatively high (as compared to vacuum) refractive indices of the materials used to fabricate CTDs (approx. 5 for Si at 400 nm) can make reflective losses a significant factor. Anti-reflection (AR) coatings can be used in the manufacture of CTDs to reduce reflective losses over a particular wavelength range. Back side illuminated CCDs are particularly amenable to AR coating. Silicon dioxide and silicon nitride have lower indices of refraction than silicon and so losses due to reflection can be

minimized by optimizing the thickness of layers of these materials when used as insulators on front side illuminated devices.

Dark Current

Modern silicon CTDs are operated at low temperatures so that the dark count rate is extremely low. For silicon array detectors, the thermally generated charge carriers are generated at midgap defects in the bulk silicon and at the surface Si-SiO_2 interface.[15] The rate of thermal charge generation can be reduced by cooling; however, CCDs can not be cooled to arbitrarly low temperatures. The ability to transfer the photogenerated charge from the individual detector sites to the input node of the on chip amplifier of the CCD decreases as the temperature is reduced giving a lower temperature limit of operation for most CCDs of approximately 150 K. Because CIDs employ intra-cell readout, high CTEs are not required and hence CIDs can be operated at lower temperatures. As can be seem from Table II, the dark count rate for these cooled CCDs is in the range of <0.001 to 0.03 electrons per detector element per second, and for CIDs the dark count rate is zero within the accuracy of the measurements (<0.008 carriers per detector element per second at 120 K).

Sensitivity

High sensitivity is critical for luminescence and other forms of low light level spectroscopy as well as low light level imaging. The CCD detector is currently the most sensitive detector available for low flux conditions. This is due to an extremely high quantum efficiency, low dark current and the lowest read noise of all integrating silicon detectors. Table III lists the theoretical minimum detectable signals in photons per detector element that

can be measured using a CCD, CID, PDA, PMT, and intensified silicon PDA (ISPDA). These calculations include the effects of detector quantum efficiency, photon shot noise, detector read noise, and assume the dark current follows Poisson statistics.[16] It should be emphasized that the comparisons are made on a detector element by detector element basis and do not include the multichannel advantage that is inherent in the multichannel detectors. As shown in Table III, the CCD has a minimum detectable signal of 0.2 photons per second per detector element at 500 nm with an integration time of 100 seconds. Note that the representative photon counting PMT is less sensitive by a factor of 5, with the least sensitive detector being the PDA. Appendix 1 contains the equations used to arrive at the results in Table III.

It is worthwhile to consider the effects of image intensification on an intrinsically sensitive detector such as a CCD or CID. The minimum signal that can be detected with a CTD or PDA is stated in terms of charge carriers. The integration time allowed for the collection of these charge carriers sets the minimum flux detectable; when long periods of time are available the minimum detectable flux can be very low. Serially interrogated CTDs and PDAs cannot be used directly in experimental situations that require fast time discrimination of the optical signal (less than several tens of microseconds). It is in these situations that intensification is advantageous. As with ISPDAs, intensification allows a CID or CCD to be used in fast time resolved spectroscopy. Unlike PDAs however, intensification does not improve the low light level sensitivity of these detectors. It is important to realize the performance trade-offs of intensification: photocathode materials generally offer a lower quantum efficiency over an extended wavelength range and have a much higher dark count rate, particularly photocathodes used in microchannel

plate image intensifiers. Intensification also reduces the dynamic range of the sensor system. Intensifiers themselves have a limited dynamic range, and because they produce multiple output events for each input event, the image detector elements reach saturation more rapidly. Thus, intensification of a CTD should only be used in situations requiring the high speed shuttering ability of microchannel plate image intensifiers.

Dynamic Range

It is fairly straightforward to determine the dynamic range of similar single channel detectors. It is much more difficult to accurately compare the dynamic ranges of multichannel detectors with differing abilities such as CIDs employing the NDRO and CCDs which allow binning. All integrating photodetectors have a simple dynamic range defined as the ratio of the maximum amount of charge that can be contained in a detector element (the saturation level) to the minimum amount of charge that can be measured (twice the read noise) or $Q_{sat}/2N_r$. This dynamic range limits the contrast of a scene that can be directly imaged. For some CCDs, binning can increase the upper end of the dynamic range while decreasing the resolution.

In the normal operation of an integrating detector, all detector elements are exposed to the source for the same length of time. In a single exposure, the dynamic range is dictated by the simple dynamic range of the detector. This exposure time can be varied over a wide range however, allowing the dynamic range to be adjusted to suit the source intensity. As an illustration of this, consider photographic emulsion, where the simple dynamic range is the dynamic range obtainable from the film. Control of the length of time the film is exposed to the source shifts the range over which intensities

can be quantified. The overall dynamic range of the system is dictated by both the dynamic range of the film and the available range of exposure times.

In the case of the Tektronix TK512M CCD described in Table II, the most intense single feature measurable corresponds to $5x10^{8}$ photons per second at 500 nm with a 1 msec. integration time. The lowest intensity measurable is $7x10^{-2}$ photons per sec. at 500 nm employing a 500 second observation time. This gives a dynamic range between the most and least intense observable features of approximately ten orders of magnitude. In practice, a series of exposures can be made at exposure times appropriate to the intensity of the source and the transient nature of the experiment. This technique of multiple exposure dynamic range enhancement has been described in the literature for photodiode arrays and has been shown to be effective in extending the dynamic range of these devices.[17] Blooming, the spilling of excess photogenerated charge from overexposed regions of a multichannel detector into adjacent regions poses two limitations on dynamic range extension through variations in integration time. First, charge is not conserved as it spills from one detector element to the next so the ability to quantify the "bloomed" spectral feature is lost. Second, charge spillage from intensely illuminated detector elements into adjacent detector elements destroys the information contained in these detector elements. Even if it is not necessary to quantify intense spectral features, their presence limits the ability to detect faint spectral features. Most CCDs bloom to some extent, and so cannot be used indiscriminately with the multiple exposure technique. Care must be taken so that the simple dynamic range of the device is not exceeded. Several CCDs have

been fabricated to include antiblooming drains which minimize this problem; however, these CCDs are not common.

Although the simple dynamic range is quite high for CCDs and PDAs as compared to other types of imagers (Vidicons etc.), they may not reach the very high values required by some analytical spectroscopies such as atomic emission spectroscopy (AES). A method exists for the extension of the upper end of the CID's dynamic range, which results in this imager being quite well suited to AES. The method is called random access integration (RAI), and involves varying the photon integration time from spectral feature to spectral feature and using the NDRO process to determine the optimum time for read out.[18,19] The photon flux at intensely illuminated regions of the detector is quantified prior to saturation, and weak signals are allowed to integrate for long periods of time to allow the highest possible SNR. A computerized system sequentially checks the signal level at each of the spectral features of interest using the NDRO while the detector is being exposed to the analytical source. The system then records the signal level and integration time of a spectral feature when the point of adequate SNR has been reached.

The RAI method employed with the CID is similar to a variable integration time (VIT) method described for use with vidicon tubes.[20-23] These detectors are also capable of random access, but do not have the NDRO capability. This introduces a prior knowledge limitation that requires that all intensely illuminated regions of the target be known in advance so that they can be prevented from blooming during the course of the exposure. Additionally, the approximate intensity of the spectral features of interest must be known so that appropriate integration times can be chosen.

An alternate variable integration time detection method has been employed with PDAs,[24,25] and is applicable to CCDs. These detectors do not allow random access nor NDROs. The VIT technique refers to a series of geometrically increasing integration time exposures (i.e. 1, 2, 4, 8 second exposures), where intense spectral features are quantified with the short exposures and faint spectral features are quantified with the long ones. Blooming in PDAs is much less severe than in vidicons, but faint spectral features adjacent to intense ones may be obscured. This is particularly a problem in AES. Blooming is not a problem with the CID employed in the RAI mode. The total time required to complete a spectral measurement with a PDA or CCD employed in this VIT mode is longer than the time required with the CID or vidicon systems, since a number of exposures are employed rather than a single one. This disadvantage is only significant in systems where time is limited.

As previously mentioned, an alternate method to achieving an extension of the dynamic range is by summing multiple exposures externally (as in computer memory), but this lowers the SNR as compared to summing charge on detector. Noise associated with reading out the detector is summed along with the signal and limits the intensity of the faint features that are observable. The SNR advantage that is possible when a single exposure is used (employing RAI or VIT detection) rather than the external sum of a number of exposures is proportional to the square root of the number of multiple exposures that are used (noise is assumed to be white).

Conclusions

Many of the characteristics of charge transfer devices which make them suitable for analytical optical spectroscopy have been described. As a class, CIDs and CCDs offer extremely high sensitivity, broad wavelength response, virtually no dark current and a very large number of detector elements, as well as availability in a large number of formats. The major advantage CIDs have over other silicon array detectors for analytical spectroscopy is the ability to perform non-destructive readouts at pseudo-randomly addressed detector elements. This allows the very powerful technique of random access integration detection to be used to extend dynamic range. Other advantages associated with the CID architecture make these devices relatively easy to fabricate, but at the current state of the art in MOS fabrication technology, these advantages are becoming relatively less important. Nevertheless, these differences result in a relatively inexpensive imager.

The refinement of CCD technology has proceeded to the point where devices approaching the theoretical limits of performance have been produced. Backside illuminated CCDs employing thin flash grown oxide layers can be anti-reflection coated to give very near 100% QE over essentially any wavelength window between 0.1 and 800 nm. Three or four phase architecture can be used to give extremely high charge transfer efficiency and on chip preamplifiers have been optimized to produce under five electrons of read noise. Formats ranging in size from a relatively small number of large detector elements to millions of detector elements are available and anti-blooming drains can be incorporated to prevent charge leakage even at very high levels of overload.

Unfortunately, (with the exception of a few experimental devices) no manufacturer has yet combined all of these technological advances into a single detector. It appears that the scientific community will have to wait a while longer for these near perfect light detectors to become available. One can only speculate as to whether or not the demand for high quality scientific imagers will increase sufficiently for a source to emerge.

Application of CIDs and CCDs in analytical spectroscopy, unlike their application in direct imaging, requires the development of unique experimental configurations rather than the direct replacement of existing detectors with new ones. It is the requirement of this additional effort that the authors believe has been partially responsible for the relatively slow acceptance of this new technology in spectrochemical analysis. For example, while the optimum use of a detector array with over four million individual detectors, each as sensitive as the most sensitive PMT, offers tremendous potential for improving many forms of spectroscopy, the design and the development of a spectrometer system to optimally utilize the power of this detector is difficult.

The second article in this series will deal with the application of integrating photo detectors (CTDs and PDAs) in spectrochemical analysis. Considerations important to the design of spectrometers which fully utilize the capabilities of CTDs will be discussed and examples of systems which employ CTD detectors will be presented. Examples of CTD based optical spectrometers currently in use or under development in our laboratories include a plasma atomic emission spectrometer using a CID, a combination absorption, fluorescence, phosphorescence spectrometer using a two dimensional CCD, a rapid scanning spectrophotometer employing a two dimensional CCD, a

holographic interferometer employing a linear CID, and an imaging spectrophotometer for the spatial mapping of the absorption spectra of optically opaque thin films.

The high sensitivity, large number of detector elements and wide dynamic range offered by modern CTDs should make them the detectors of choice in the future for a large number of analytical applications. The authors anticipate the reporting of a large number of new instrumental configurations devised to utilize CTDs, as well as the application of CTD-based detector systems, to be the solution of a number of analytical problems.

Acknowledgement

The authors wish to thank Richard Aikens of Photometrics Ltd., Tucson, AZ, for many useful discussions concerning the operation and application of CCDs. This research was partially supported by the Office of Naval Research.

References

1. D.F. Barbe and S.B. Campana, "Imaging Arrays Using the Charge-Coupled Concept," in Advances in Image Pick-up and Display, B. Kazan, Ed. (Academic Press, New York, 1977), Vol. 3, Chap. 3.

2. P.K. Weimer and A.D. Cope, "Image Sensors for Television and Related Applications," in Advances in Image Pick-up and Display, B. Kazan, Ed. (Academic Press, New York, 1983), Vol. 6, Chap. 3.

3. E.L. Dereniak and D.G. Crowe, Optical Radiation Detectors (John Wiley, New York, 1984), Chap. 9.

4. See J. Opt. Eng. Vol. 41, Nos. 7, 8, and 9 (1987).

5. G.J. Michon, H.K. Burke and P.M. Brown, "Recent Developments in CID Imaging," in Proceedings of Symposium on Charge-Coupled Device Technology for Scientific Imaging Applications (Jet Propulsion Laboratory, Pasadena, CA, 1975), p. 106.

6. J.W. Lunde, G.J. Michon and J. Carbone, 12th International Television Symposium, Symposium Record Equipment Inovations Sessions, Montreux, Switzerland, 30 May, 1981.

7. H.A. Lewis and M.B. Denton, J. Auto. Chem. 3, 9, (1981).

8. S.R. Sims and M.B. Denton, "Multielement Emission Spectrometry Using a Charge-Injection Device Detector," in Multichannel Image Detectors, Y. Talmi, Ed. ACS Symposium Series No. 236, 1981) Vol. 2, Chap. 5.

9. S.R. Sims and M.B. Denton, J. Opt. Eng., (1987), in press.

10. W.S. Boyle, and G.E. Smith, Bell System Technical Journal 49, 587 (1970).

11. G.F. Amelio, M.F. Tompsett and G.E. Smith, Bell Systems Technical Journal 49, 593 (1970).

12. J.R. Janesick, T. Elliott, S. Collins, H. Marsh, M. Blouke, and J. Freeman, "The Future Scientific CCD," in State-of-the-Art Imaging Arrays and Their Applications, K. Prettyjohns, Ed., Proc. SPIE 501,2 (1984).

13. J. Janesick, D. Campbell, T. Elliott, T. Daud, P. Uttley, "Flash Technology for imaging in the UV," in UV Technology, R. Huffman ed., Proc. SPIE 687, 36 (1986).

14. R.K. Hopwood, "Design Considerations for a Solid-State Image Sensing System" in Minicomputers and Microprocessors in Optical Systems, C.S. Koliopoulos, F.M. Zweibaum ed., Proc. SPIE 230, 188 (1980).

15. N.S. Saks, J. Appl. Phys. 53, 1745 (1982).

16. R.B. Bilhorn, P.M. Epperson and M.B. Denton, Spectrochim. Acta (1987), in prep.

17. Y. Talmi and R.W. Simpson, Appl. Optics 19, 1401 (1980).

18. R.B. Bilhorn and M.B. Denton, Appl. Spectros. (1987), in prep.

19. R.B. Bilhorn and M.B. Denton, Anal. Chem. (1987), in prep.

20. D.G. Mitchell, K.W. Jackson and K.M. Aldous, Anal. Chem. 45, 1215A (1973).

21. D.L. Wood, A.B. Dargis and D.L. Nash, Appl. Spectros. 39, 310 (1975).

22. T.A. Nieman and C.G. Enke, Anal. Chem. 48, 619 (1976).

23. S.S. Vogt, R.G. Tull and P. Kelton, Appl. Opt. 17, 574 (1978).

24. G. Horlick, Appl Spectros. 30, 113 (1976).

25. Y. Talmi and R.W. Simpson, Appl. Opt. 19, 1401 (1980).

Table I. Formats of Representative Charge Transfer Devices

Manufacturer	Imager (model #)	Dimensions (active elements)	Detector Size (microns)	Overall Photo-active Area (mm)
General Electric	CID11B	244 by 248	47 by 35	11.5 by 8.7
General Electric	CID17B	244 by 378	27.2 by 23.3	6.5 by 8.7
General Electric	CID35	512 by 512	14 by 14	7.2 by 7.2
General Electric	CID75	1 by 1	1000 by 1000	1 by 1
General Electric	CID62	512 by 32	29 by 127	14.8 by 4.1
Texas Instruments	VP800R	800 by 800	15 by 15	12 by 12
Texas Instruments	VP1M	1024 by 1024	18 by 18	18.4 by 18.4
Texas Instruments	TC104	3456 by 1	10.3 by 10.3	35.6 by 0.01
RCA	SID501EX	512 by 320	30 by 30	15.4 by 9.6
RCA	SID504DD	256 by 403	19 by 16	4.8 by 6.5
Tektronix	TK512M	512 by 512	27 by 27	13.8 by 13.8
Tektronix	TK2048M	2048 by 2048	27 by 27	55.3 by 55.3
Thomson-CSF	TH7882CDA	384 by 576	23 by 23	8.8 by 13.2
Kodak	M1A	1320 by 1035	6.8 by 6.8	9.0 by 7.0

Table II. Electro-optical Characteristics of Selected CTDs

Device	Architecture	Dimensions (elements)	Peak QE (%) wavelength	Range over which QE exceeds 10%	full well (carriers)	noise (carriers)	notes
RCA[a] SID501EX	CCD, 3-phase back-side	512 by 320	95% at 500 nm	200[b] - 950 nm	$4x10^5$	50	AR coating for 500
Tektronix[c] TK512M-011	CCD, 3-phase front-side	512 by 512	35% at 750 nm	450 - 950 nm	$9x10^5$	6	
Texas Instruments[d]	CCD, 3-phase back-side	800 by 800	90% at 550 nm	0.1[b] - 1050 nm	$5x10^4$	5	optimized process Prototype AR coating for 550
Texas Instruments[a] TC104-1	CCD, uniphase front-side	3456 by 1	95% at 400 nm	200[b] - 1000 nm	$3x10^5$	80	No gates over photoactive region. AR coated for 400 nm
General Electric[e] CID17-B	CID	244 by 388	47% at 550 nm	210 - 850 nm	$6x10^5$	60	
General Electric[f] CID75	CID	1 by 1	35% at 250 nm	200[b] - 850 nm	$1x10^8$	80	prototype devices

(a) Measurements made in these laboratories. (b) Point at which QE measurements stopped. QE may exceed 10% beyond this point. (c) P.M. Epperson, J.V. Sweedler, M.B. Denton, G.R. Sims, T.W. McCurnin, R.S. Aikens, J. Opt. Eng. 41, (1987), in press. (d) ref. 13. (e) ref. 17. (f) J.V. Sweedler, M.B. Denton, G.R. Sims, R.S. Aikens, J. Opt. Eng. 41, (1987), in press.

Table IIIA. Comparison Between the minimum Detectable Signal of a PDA, ISPDA, CID, PMT and CCD[a]

Signal Acquisition Time (sec)	Minimum detectable signal (SNR=2), photons per second per detector element									
	PDA		ISPDA		CID		PMT		CCD	
	UV	VIS	UV	VIS	UV	VIS	UV	VIS	UV	VIS
1	6000	3300	1230	2100	420	330	30	122	31	17
10	671	363	390[b]	660[b]	41	32	6.3	26	3.1	1.7
100	112	62	123[b]	210[b]	4.2	3.3	1.8	7.3	0.3	0.2

Table IIIB. Parameters Used in Calculating the Minimum Detectable Signal

Parameter	PDA[c]	ISPDA[d]	CID[e]	PMT[f]	CCD[g]
QE at 600 nm	73%	6%	37%	5%	84%
QE at 300 nm	40%	10%	19%	21%	50%
Dark count rate[h]	36,000 (e^-/sec)	<4000 (counts/sec)	<0.008 (+/sec)	3 (counts/sec)	<0.001 (e^-/sec)
Read Noise	1200 e^-	<1 count	60 +	0	6 e^-

(a) Noise contributions due to photon shot noise, dark count shot noise, and read noise have been included. Noise contributions from source or detector fluctuations (1/f type) are not included. See Appendix 1. (b) The ISPDA nas a limited dynamic range and so ten one second exposures are averaged for the ten second acquisition time, and 100 for the 100 second acquisition time. (c) Reticon model RL-1024S PDA. Data from Y. Talmi, Appl. Spec. 36, 1, 1982 and ref. 17. (d) PAR model 1421B-1024-G microchannel plate intensified PDA, EG&G Princeton Applied Research, Princeton, New Jersey 08540, and from Y. Talmi, Appl. Spec. 36,1, 1982 (Table VII p. 15). The results obtained here for the ISPDA are in contrast to those reported in the last ref. (e) CID17-B, ref. 18. (f) 7500-5303 photon counting PMT, Galileo Electo-Optics Co., Sturbridge, MA, 01518. (g) Antireflection coated Texas Instruments three phase back-side illuminated 800 by

800 CCD with flash gate, ref. 12,13. (h) These are the dark current rates observed at the temperatures used in the cited literature. The dark count rate of the PDA can be reduced significantly by cooling below -20 C. The dark count rate of photocathodes can not be reduced significantly by further cooling.

13) TI 4849 580 x 390

14) GE CID75 single element

Figure Captions:

Fig. 1. A detector element in a hypothetical CID. (a) Top view showing column and row electrodes. (b) Cross section showing the potential wells formed when the electrodes are biased for charge integration. The electrode biases are relative to the substrate. The + symbols represent photogenerated holes.

Fig. 2. Structure of a detector element in a modern CID. (a) Top view of a four detector element area. (b) Cross section taken through a row showing charge injection in the left detector element and charge readout in the right detector element.

Fig. 3. Readout scheme used to quantify the amount of photogenerated charge in an individual detector element of the CID. (a) The CID is in the charge integration mode. (b) The first of two measurements of the potential at the charge amplifier is performed. (c) The second measurement of potential after the charge has been moved to the row electrode is performed. The readout sequence can be completed by shifting the charge back to the column electrode as shown in (a), a nondestructive readout (NDRO), or by injecting the charge into the substrate as shown in (d), a destructive readout (DRO).

Fig. 4. Schematic representation of a CID array detector showing the row and column electrodes and two scanners. The scanners sequentially connect rows and columns to the output amplifier and charge drive signal.

Fig. 5. Cross section of a hypothetical CCD detector at four different time states showing the transfer of photogenerated charge. Stored pnotogenerated electrons are transfered by application of the wave forms shown in the bottom of the figure to the three phases.

Fig. 6. Layout of a typical three phase CCD. Photogenerated charge is shifted in parallel to the serial register. The charge in the serial register is then shifted to the amplifier.

Fig. 7. Illustration of the four types of gate structures and the associated potential well diagrams used in CCDs to accomplish charge transfer: (a) Uniphase or virtual phase. The implantations introduce steps into the potential profile which force the desired charge movement as the voltage of the single electrode is raised and lowered. (b) Two phase. Steps in the potential wells force the desired charge movement as the two phases are clocked with complementary square waves. (c) Three phase. The actual gate structure used to achieve the operation illustrated in figure 4. (d) Four phase. Charge is shifted by sequentially applying a low voltage to the four electrodes one at a time.

Fig. 8. Several of the CTDs used in these laboratories.

1) Tektronix TK 2048M 2048 x 2048
2) English Electric Valve P8602 580 x 390
3) RCA 504DD 256 x 403
4) GE CID17 244 x 378
5) RCA 501EX 512 x 320
6) Thomson CSF TH7882 576 x 384 w/fiber bundle
7) Thomson CSF TH7803 1 x 1728
8) GE CID62 512 x 32
9) TI TC104 3456 x 1
10) TI TC101 1728 x 1
11) GE CID 128 x 128
12) GE CID11B 244 x 248
13) TI 4849 580 x 390
14) GE CID75 single element

Appendix 1

SNR Equations Used for the Low Light Level Comparison of Spectroscopic Detectors

This appendix describes the equations used to calculate the SNR of CTDs, PDAs and PMTs under low flux conditions. Photons from a Poisson source are assumed to be incident on the detector resulting in a signal, after subtraction of any dark current, given in counts by,

$$S = n\Phi t \tag{1}$$

where n = the detector quantum efficiency or the probability that a photon will interact to produce a detectable event, Φ = the photon flux and t = the flux interaction time. For a PMT, the principle noise sources are the shot noise in the incident photon stream and the shot noise in the dark current,

$$N_{pmt} = [t(n\Phi + \Phi_D)]^{1/2} \tag{2}$$

where Φ_D is the mean dark current count rate. The overall SNR for a PMT is

$$SNR_{PMT} = \frac{n\Phi t}{[t(n\Phi + \Phi_D)]^{1/2}} \quad . \tag{3}$$

Solving eqn. 3 for the photon flux at a given SNR results in,

$$\Phi = \frac{SNR^2 + SNR(SNR^2 + 4t\Phi_D)^{1/2}}{2n^t} \quad . \tag{4}$$

Solid state silicon imagers have a finite read noise (N_r) which contributes to the noise expression of eqn. 2 to give an overall SNR expression given by,

$$SNR_{,CTD} = \frac{n\phi^{t}}{(N_r^{2} + t(n\phi + \phi_D))^{1/2}} \quad . \qquad (5)$$

Solving this equation for flux, and neglecting the dark current term results in,

$$\phi = \frac{SNR^2 + SNR(SNR^2 + 4N_r^{2})^{1/2}}{2nT} \quad . \qquad (6)$$

Defining the minimum detectable photon flux as one where SNR=2, eqns. 4 and 6 can be used to compare PDAs, PMTs and CTDs under low light level conditions.

When a microchannel plate (MCP) is used for image intensification, the quantum efficiency and dark current of the photocathode of the intensifier are used in eqn. 4. The high gain of an intensifier makes dark current and read noise from the silicon detector insignificant compared to the low QE and high dark current of the MCP. As an example, the PAR 1421R-1024 ISPDA has a 10 percent QE at 300 nm, a dark count rate of 4000 photoelectrons per second, and equivalent to one photoelectron of read noise. Using eqn. 4, the minimum detectable flux for a SNR of 2 is 1230 photons per second for a one-second observation time.

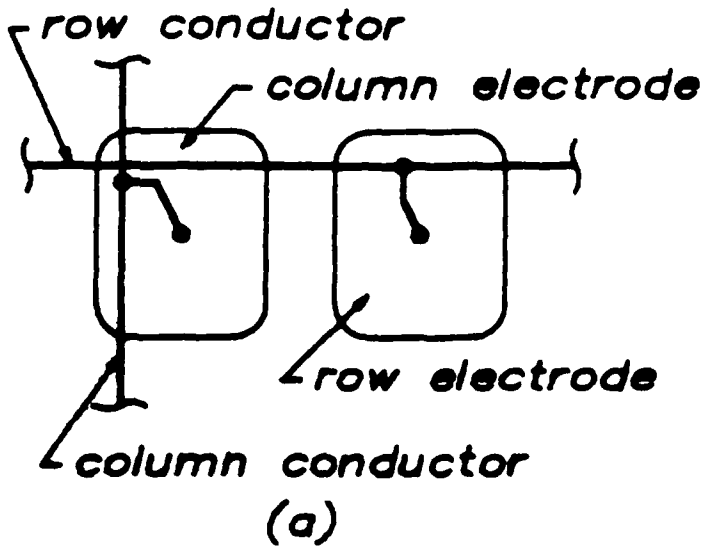
row conductor
column electrode
row electrode
column conductor

(a)

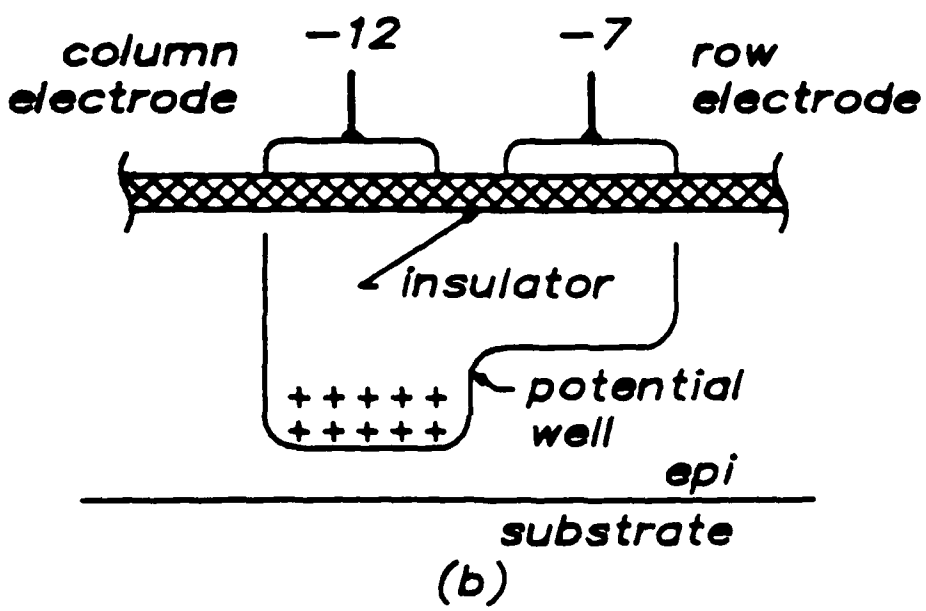
column electrode
−12
−7
row electrode
insulator
potential well
epi
substrate

(b)

Figure 1

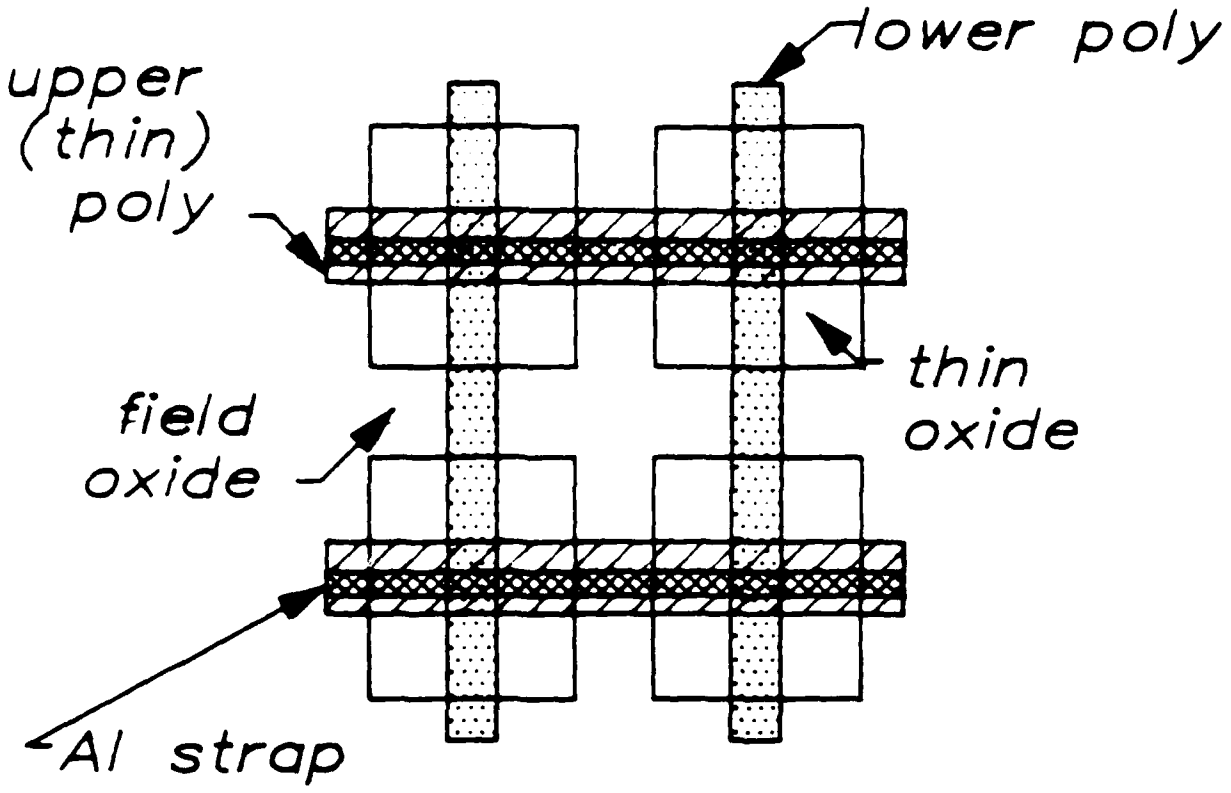
lower poly
upper (thin) poly
thin oxide
field oxide
Al strap

(a)

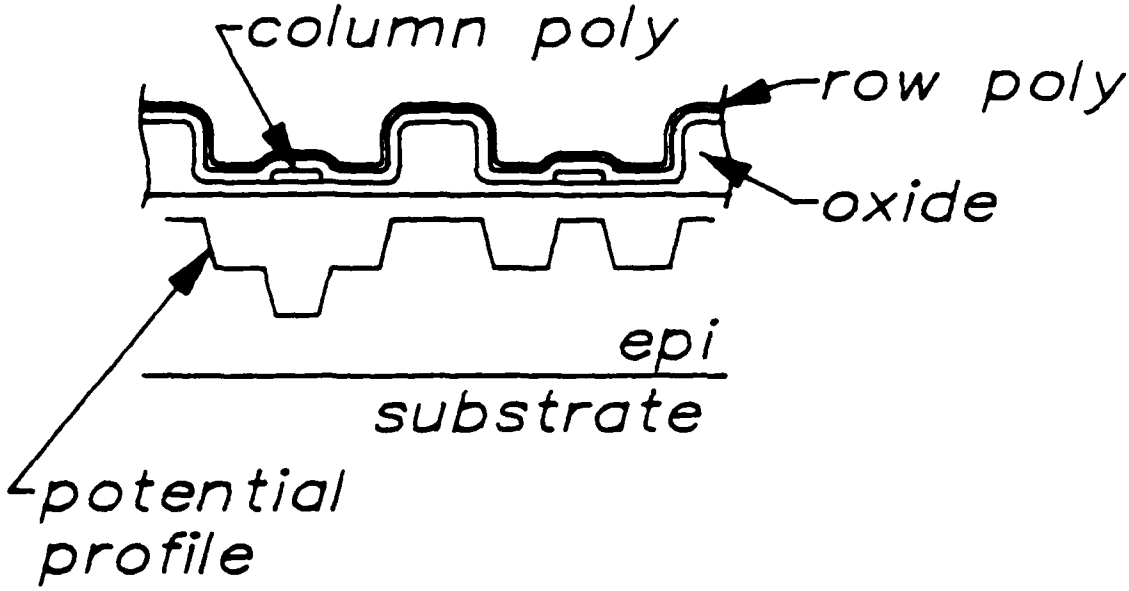
column poly
row poly
oxide
epi
substrate
potential profile

(b)

Figure 2

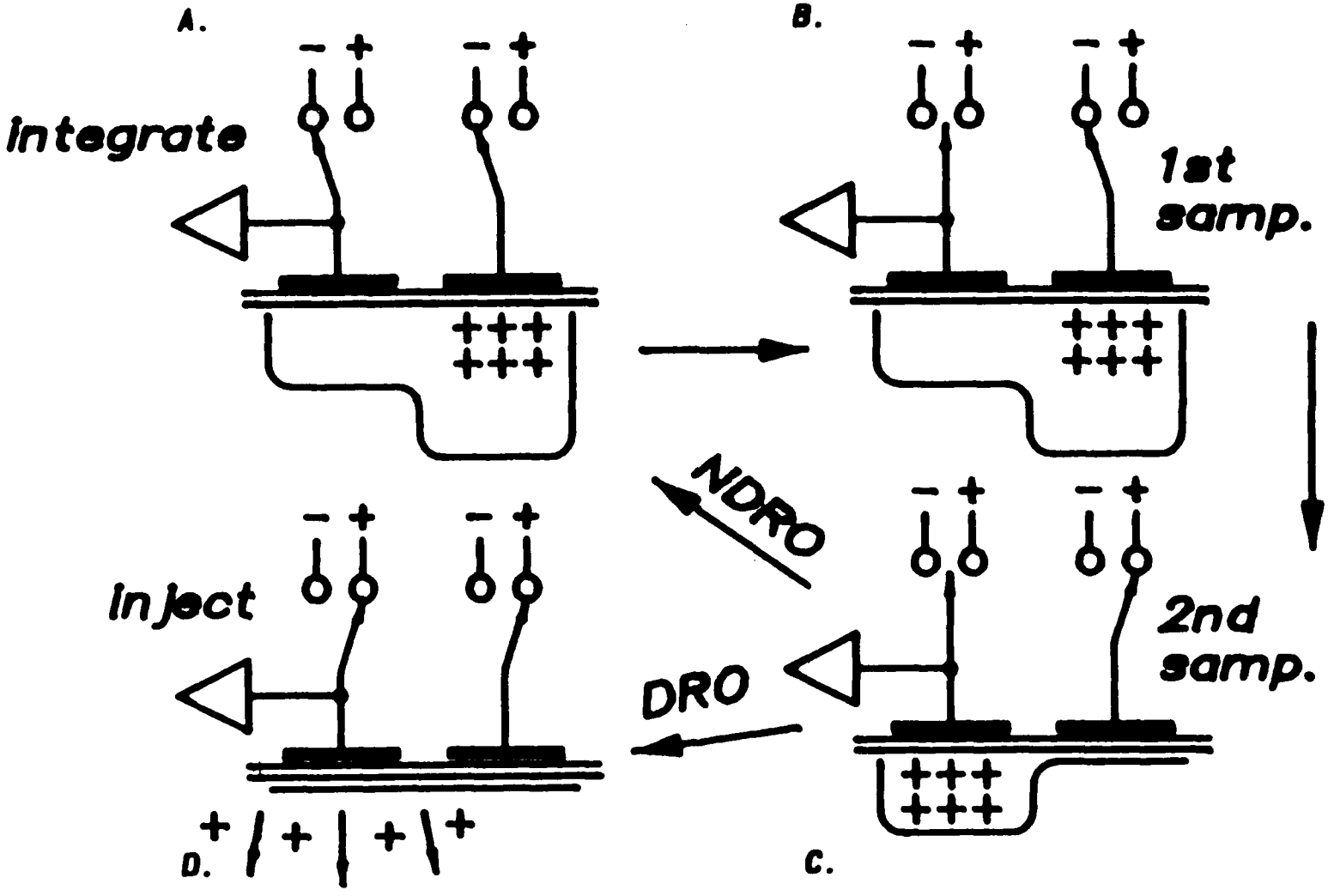

Figure 3

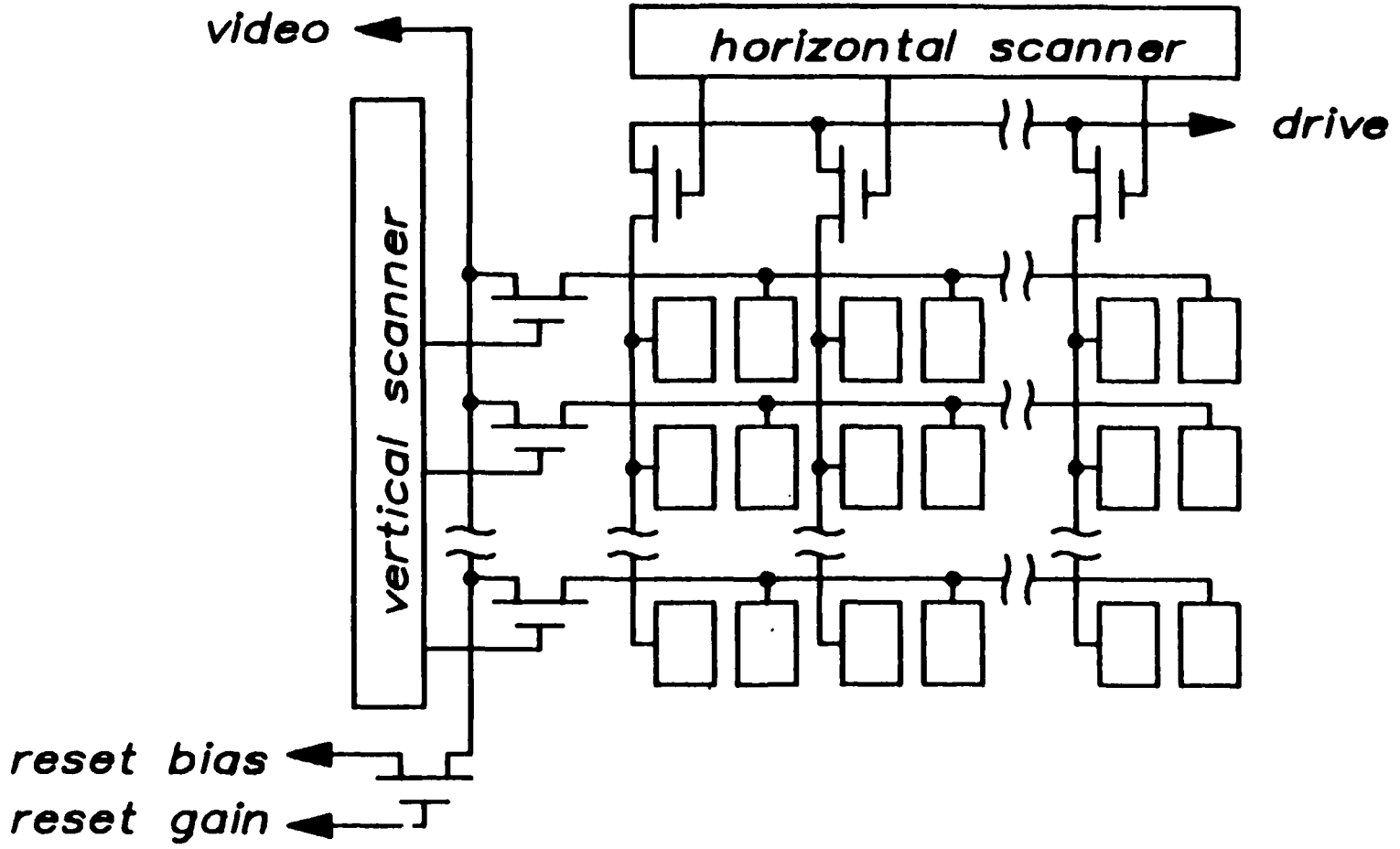
video
horizontal scanner
drive
vertical scanner
reset bias
reset gain

Figure 4

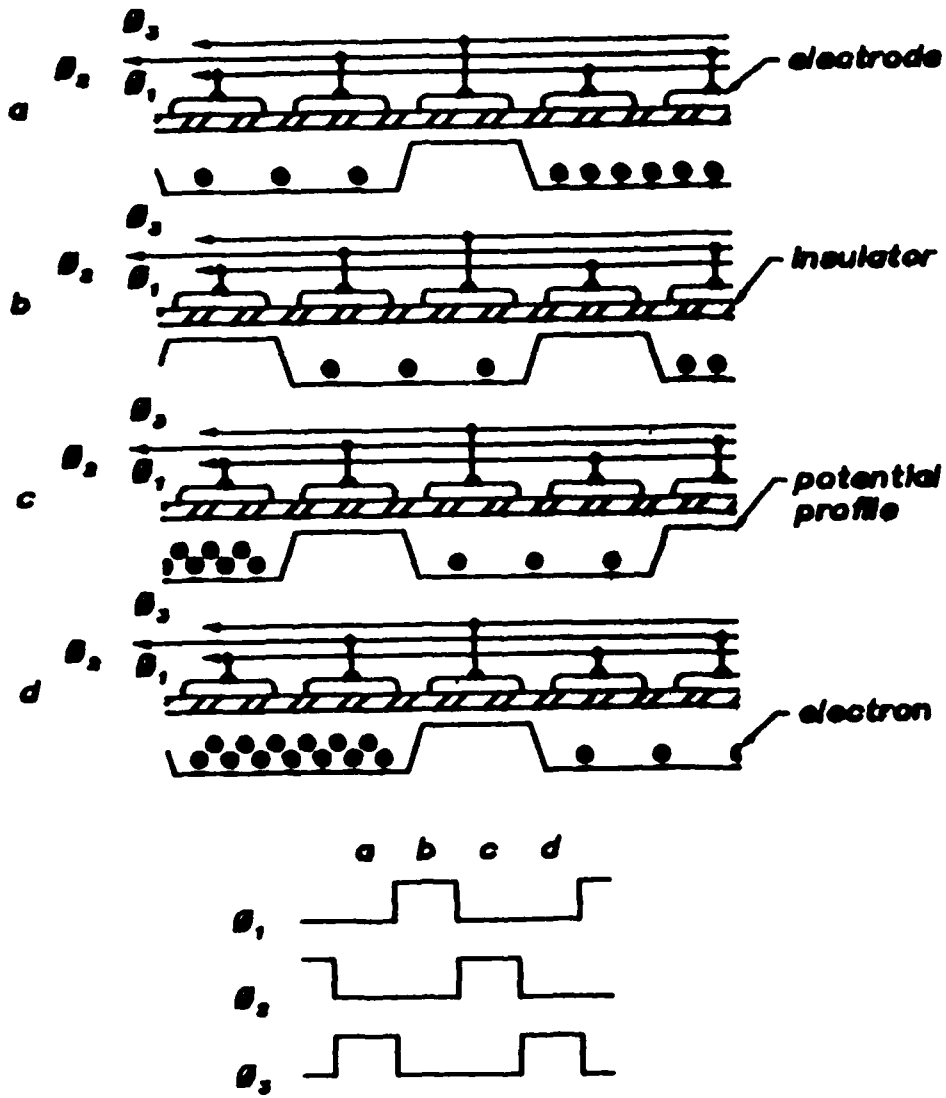
a
b
c
d
electrode
insulator
potential profile
electron
a b c d

Figure 5

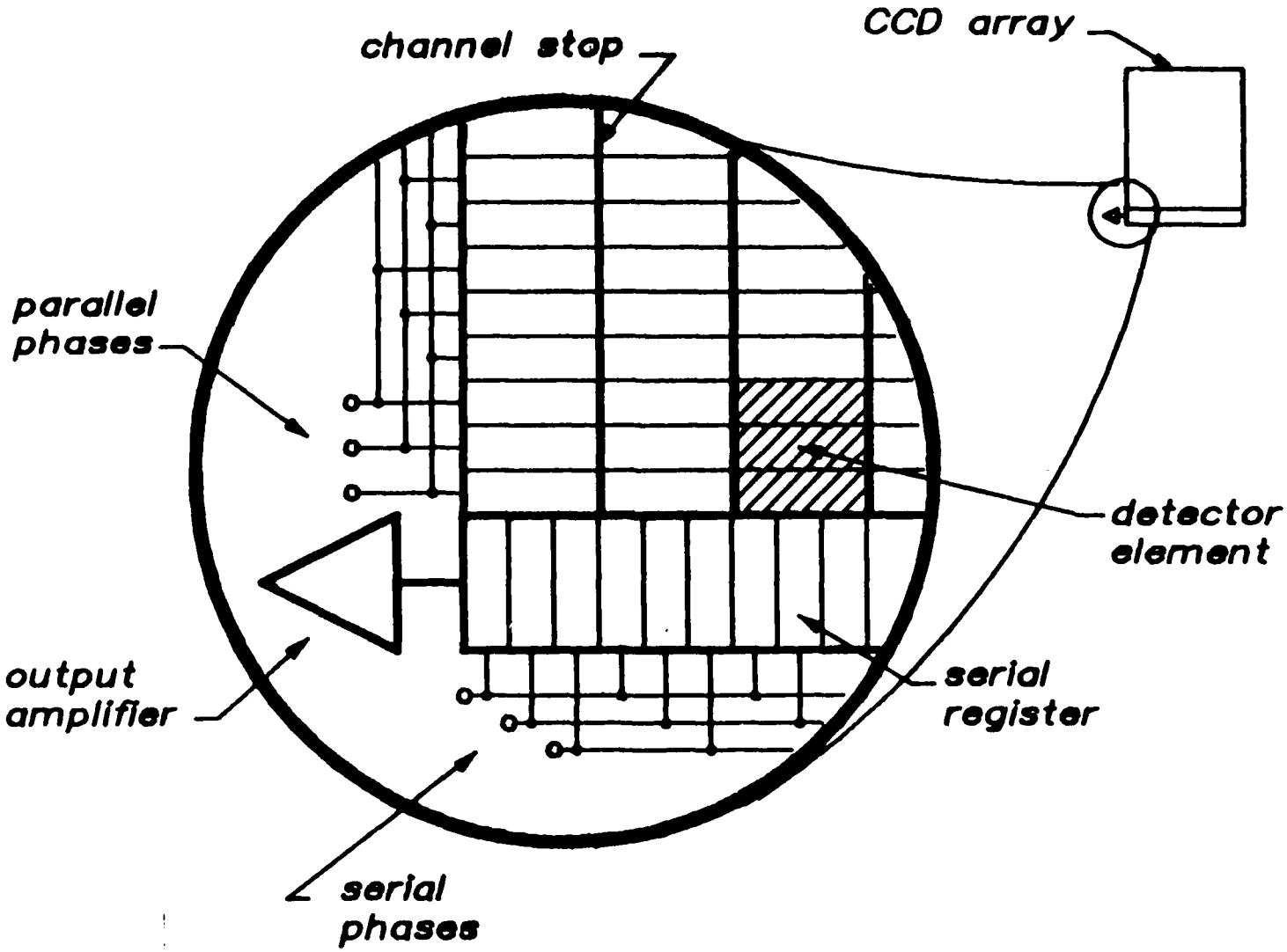
CCD array
channel stop
parallel phases
detector element
output amplifier
serial register
serial phases

Figure 6

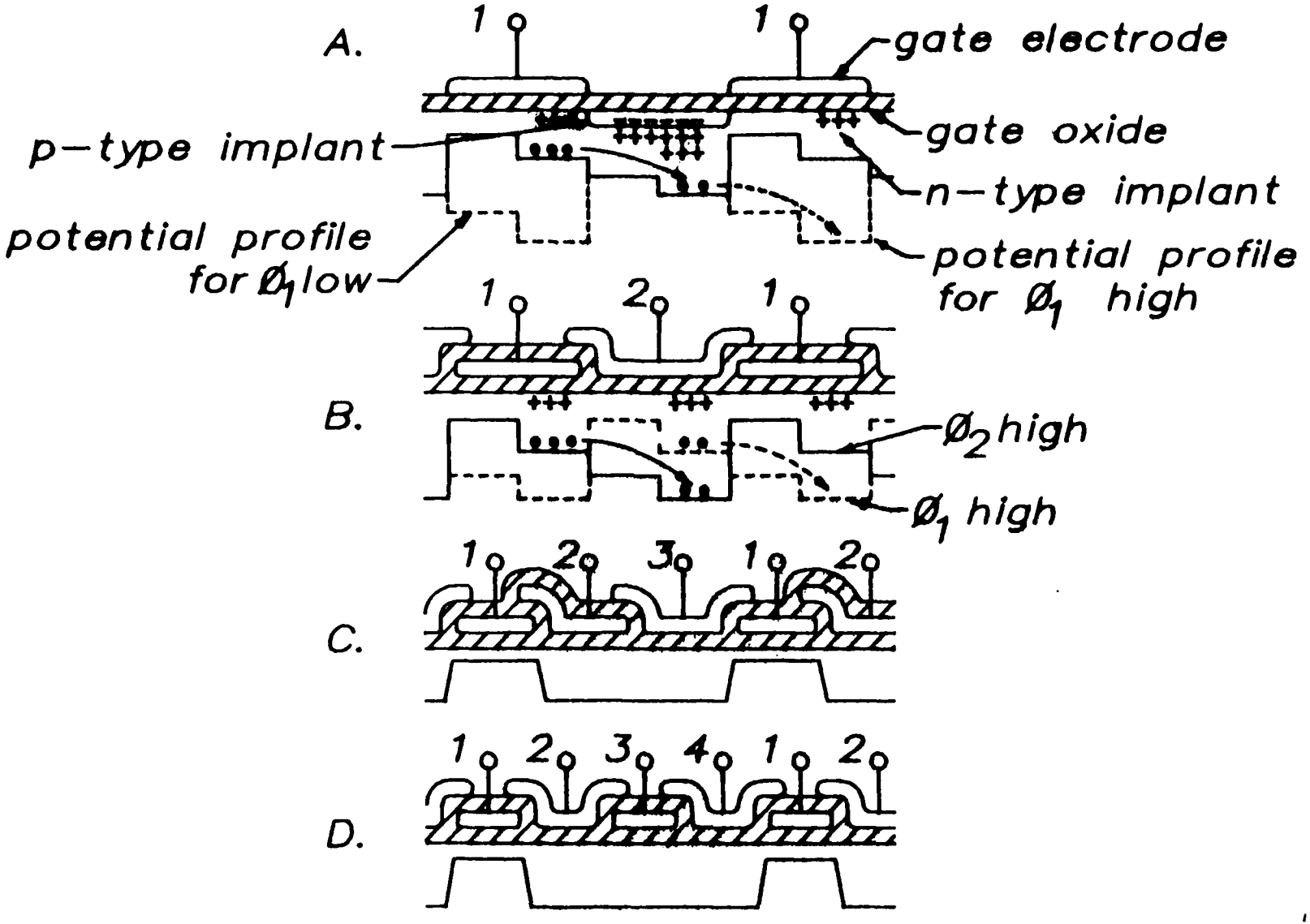
A.
1
1
gate electrode
gate oxide
p-type implant
n-type implant
potential profile
for ϕ_1 low
potential profile
for ϕ_1 high
B.
1
2
1
ϕ_2 high
ϕ_1 high
C.
1
2
3
1
2
D.
1
2
3
4
1
2

Figure 7

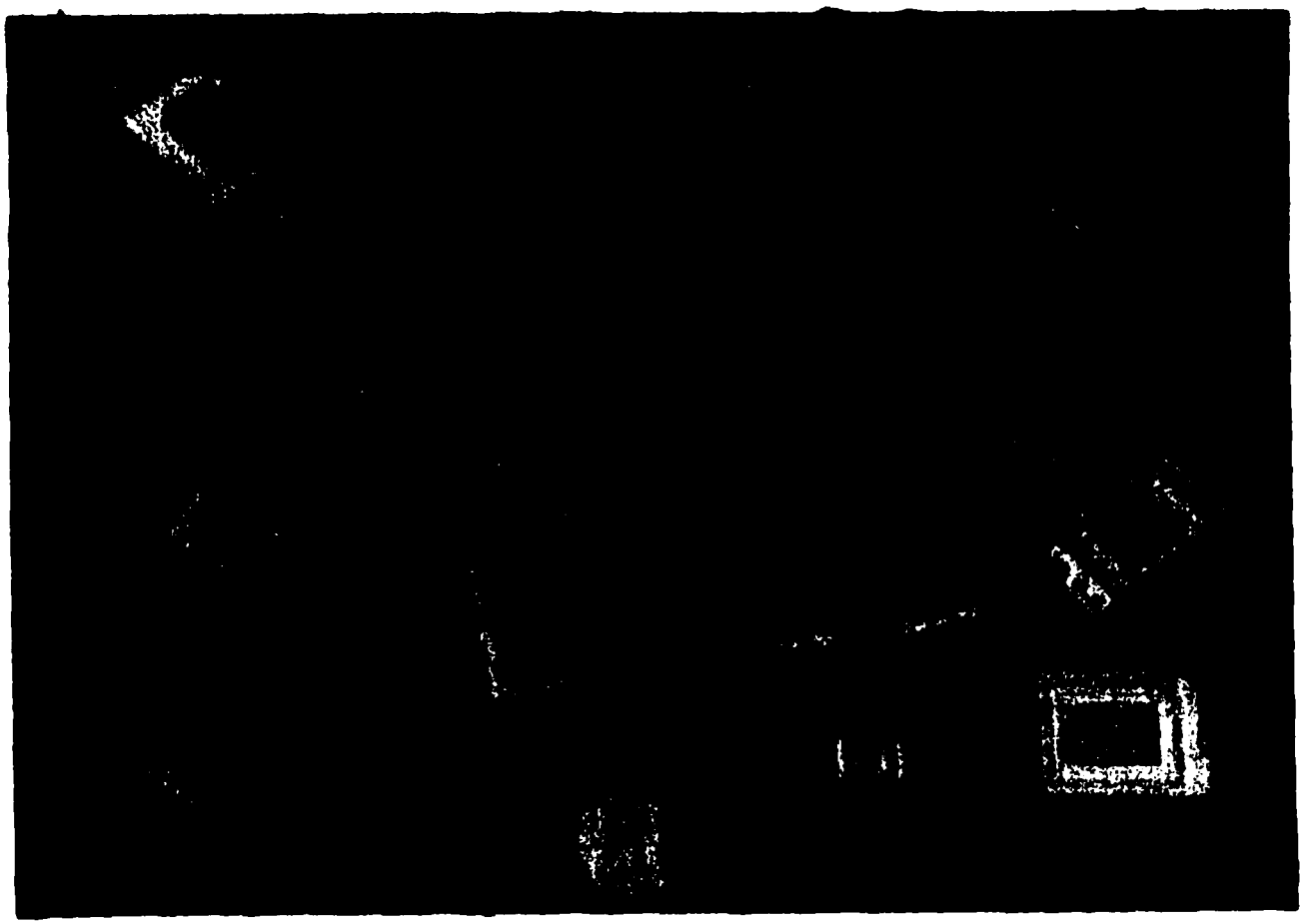

Figure 8

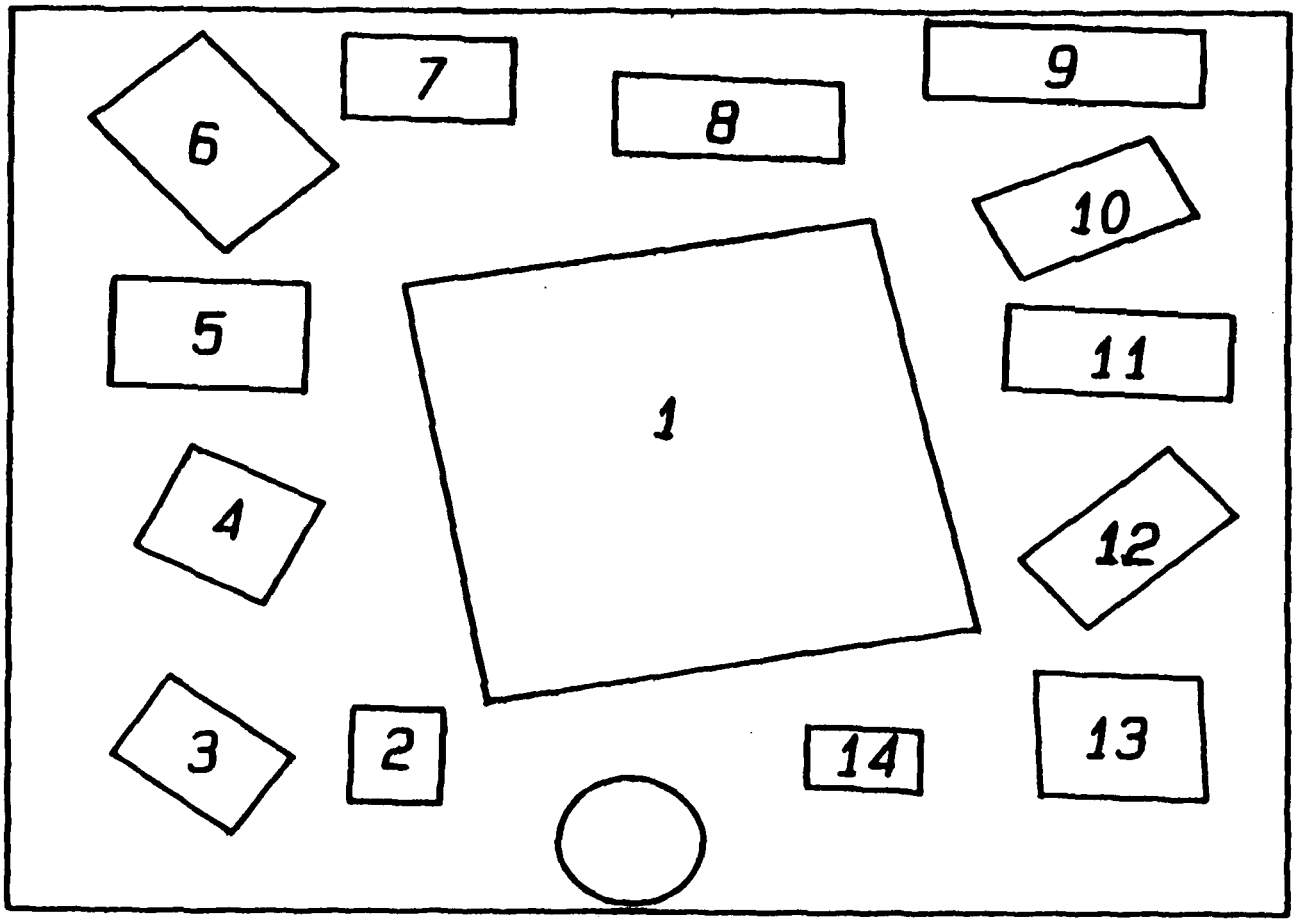

Figure 8 legend

TECHNICAL REPORT DISTRIBUTION LIST

	No. Copies
Office of Naval Research Attn: Code 413 800 N. Quincy Street Arlington, Virginia 22217	2
Dr. Bernard Douda Naval Weapons Support Center Code 5042 Crane, Indiana 47522	1
Commander, Naval Air Systems Command Attn: Code 310C (H. Rosenwasser) Washington, D.C. 20360	1
Naval Civil Engineering Laboratory Attn: Dr. R. W. Drisko Port Hueneme, California 93401	1
Defense Technical Information Ctr. Building 5, Cameron Station Alexandria, Virginia 22314	12
DTNSRDC Attn: Dr. G. Bosmajian Applied Chemistry Division Annapolis, Maryland 21401	1
Dr. William Tolles Superintendent Chemistry Division, Code 6100 Naval Research Laboratory Washington, D.C. 20375	1
Dr. David Young Code 334 NORDA NSTL, Mississippi 39529	1
Naval Weapons Center Attn: Dr. Ron Atkins Chemistry Division China Lake, California 93555	1
Scientific Advisor Commandant of the Marine Corps Code RD-1 Washington, D.C. 20380	1
U.S. Army Research Office Attn: CRD-AA-IP P.O. Box 12211 Research Triangle Park, NC 27709	1
Mr. John Boyle Materials Branch Naval Ship Engineering Center Philadelphia, Pennsylvania 19112	1
Naval Ocean Systems Center Attn: Dr. S. Yamamoto Marine Sciences Division San Diego, California 91232	1

END

9-87

DTIC